Pseudo Rotary Resonance Relaxation Dispersion Effects in Isotropic Samples

Authors: *Evgeny Nimerovsky*, Jonas Mehrens & Loren B. Andreas**

Affiliations:

Department of NMR based Structural Biology, Max Planck Institute for Multidisciplinary Sciences, Am Faßberg 11, Göttingen, Germany

*Corresponding authors: land@mpinat.mpg.de ORCID: 0000-0003-3216-9065 and evni@mpinat.mpg.de ORCID: 0000-0003-3002-0718.

Abstract

Enhanced transverse relaxation near rotary-resonance conditions is a well-documented effect for anisotropic solid samples undergoing magic-angle spinning (MAS). We report transverse signal decay associated with rotary-resonance conditions for rotating liquids, a surprising observation, since first-order anisotropic interactions are averaged at a much faster timescale as compared with the spinning frequency. We report measurements of ^{13}C and ^{1}H signal intensities under spin-lock for spinning samples of polybutadiene rubber, polyethylene glycol solution and 99.96% D_2O. A drastic reduction in spin-lock signal intensities is observed when the spin-lock frequency matches one or two times the MAS rate. In addition, oscillations of the signal are observed, consistent with a coherent origin of the effect, a pseudo rotary-resonance relaxation-dispersion (pseudo-RRD). Through simulations, we qualitatively describe the appearance of pseudo-RRD, which can be explained by time dependence caused by sample rotation and an

inhomogeneous field, the origin of which is an instrumental imperfection. Consideration of this effect is important for MAS experiments based on rotary-resonance conditions, and motivates the design of new MAS coils with improved rf-field homogeneity.

KEYWORDS: Magic-angle spinning, nuclear magnetic resonance spectroscopy, pseudo rotary-resonance relaxation-dispersion effect

Introduction

Measurement of the transverse relaxation rates of nuclear spins as a function of the applied rf-field spin-lock strengths is an elegant and well-established method for detecting structural molecular dynamics.(Abyzov et al., 2022; Alam et al., 2024; Camacho-Zarco et al., 2022; Hu et al., 2021; Massi and Peng, 2018; Palmer, 2015; Palmer and Massi, 2006; Pratihar et al., 2016; Rangadurai et al., 2019; Sekhar and Kay, 2019; Stief et al., 2024) For molecular solids, rocking motion or slow exchange in organic and inorganic samples(Fonseca et al., 2022; Keeler and McDermott, 2022; Krushelnitsky et al., 2018, 2023; Kurauskas et al., 2017; Lewandowski et al., 2011; Ma et al., 2014; Marion et al., 2019; Öster et al., 2019; Quinn and McDermott, 2009; Rovó and Linser, 2018; Shcherbakov et al., 2023; Vugmeyster et al., 2023) under MAS(Andrew et al., 1958; Lowe, 1959) NMR have been studied via the impact on transverse relaxation. This detection can be achieved by performing a spin-lock experiment,(Furman et al., 1998) where the decay of magnetization is measured as a function of the power of the applied spin-lock (SL) pulse. For slow motion or slow exchange in the microsecond (μs) range, the spectral densities(Redfield, 1957) of the investigated spins may include additional terms(Kurbanov et al., 2011; Marion et al., 2019) that arise from non-averaged anisotropic interactions.(Kurbanov et al., 2011; Rovó, 2020; Schanda and Ernst, 2016) These terms depend on the sums and differences between the nutation frequency induced by the rf-field ($\nu_{SL}=\gamma B_1/(2\pi)$) and MAS rate ($\nu_R$). Such

dependence causes a significant increase in the measured relaxation rates when ν_{SL} approaches

one of the rotary-resonance conditions ($\nu_{SL} = \nu_R$ or $2\nu_R$).(Marion et al., 2019)

For liquid samples, where SL experiments are routinely used to detect fast exchange,(Cavanagh

et al., 2006; Deverell et al., 1970; Palmer, 2004) sample rotation is not expected to induce any

rotary-resonance conditions based on anisotropic spin interactions,(Levitt et al., 1988; Oas et al.,

1988) since such interactions are eliminated by nanosecond-timescale isotropic

motion.(Haeberlen and Waugh, 1968; Maricq, 1982) However, to our surprise, we still observed

changes in the SL signals at rotary-resonance conditions for liquid and liquid-like samples during

SL experiments. Since the signal decreases, but is also clearly oscillatory, a signature of coherent

effects, we refer to this phenomenon as a pseudo rotary-resonance relaxation-dispersion (pseudo-

RRD). A review of the literature revealed articles suggesting related resonance conditions for

rotating liquid samples: in adiabatic TOCSY experiments, enhanced performance was observed

under specific matching conditions in relation to the spinning frequency.(Kupče et al., 2001;

Zektzer et al., 2005)

In this article, we measured pseudo-RRD for several liquid and liquid-like samples, and observe

similar effects in each. Through numerical simulations,(Nimerovsky and Goldbourt, 2012) we

show that this behavior can be qualitatively explained by the influence of the periodic component

of the applied rf-field, which arises from the rotation of the sample in a spatially inhomogeneous

rf-field.(Aebischer et al., 2021; Tošner et al., 2017)

Results and Discussion

We measured pseudo RRD for natural abundance ^{13}C polybutadiene rubber at 10 kHz, 20

kHz and 35 kHz MAS. The same pseudo RRD behavior is observed for a polyethylene glycol

Figure 1 displays the spin-lock sequence. Similar to previously proposed

versions,(Vugmeyster et al., 2022) it contains a heat compensation block(Wang and Bax, 1993)

(HC), followed by a $\pi/2$-pulse, T_2 −filter(Schmidt-Rohr et al., 1992) (to reduce any broad signal

components from the polymer) and a spin-lock pulse (SL). The mixing times for HC and SL

pulses were the same during a single experiment ($t_{HC} = t_{SL} = N_{SL}T_R$), while the sum of the rf-

field powers of these applied pulses always equaled to a fixed value. In all experiments, we used

continuous HC and SL (Figure 1B) except in one (the data is shown in Figure 2C), where we

applied windowed pulses (Figure 1B). During acquisition, WALTZ16 decoupling(Shaka et al.,

1983) was used.
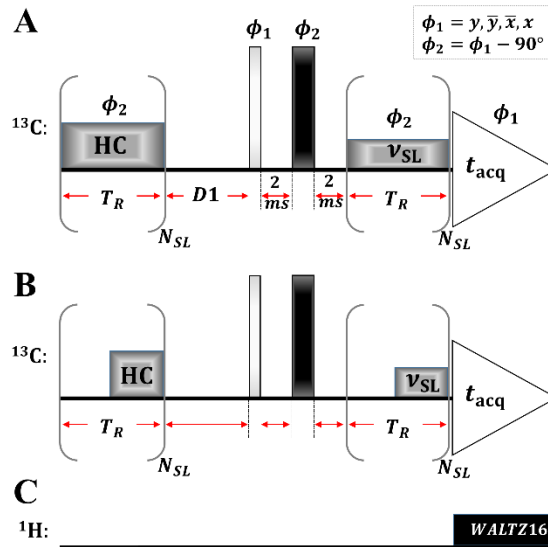
1   **Figure 1** Spin-lock sequence with heat compensation (HC), T_2 −filter (2 ms – π-pulse – 2ms) and spin-lock (SL)

2   blocks. The SL and HC elements consisted of a train of N_{SL} rotor-synchronized continuous (A) or windowed (B)

3   pulses with the same phase (ϕ_2) and rf-field strength (ν_{SL}). In all experiments, $power_{HC} + power_{SL}$ =constant

4   (equivalent to 50 kHz rf-field strength). During acquisition, WALTZ-16 decoupling(Shaka et al., 1983) (C) was

5   applied on the ^{1}H channel.

6   The experimental ^{13}C polybutadiene rubber SL profiles (acquired with a 1.3 mm probe)

7   under three different MAS rates: 10 kHz (A and C), 20 kHz (D) and 35 kHz (B) are shown in

8   Figure 2. For Figures 2A, 2B and 2D, a drastic reduction in the SL signal is observed at rotary-

9   resonance conditions when ν_{SL} equals either ν_R or $2\nu_R$. Together with reduction in the SL signal,

10   oscillations are observed. For Figure 2C, we used 10 kHz MAS and windowed pulses: half of the

11   rotor period is a window, as shown in Figure 1B. Again, a drastic reduction in the SL signal is

12   observed, but when ν_{SL} equals either to $2\nu_R$ or $4\nu_R$. We previously observed similar behavior for

13   windowed CP profiles,(Nimerovsky et al., 2023) where increasing the window between rotor-

14   synchronized pulses from zero to half a rotor period doubled the required rf-field strength for

15   cross-polarization transfers.(Hartmann and Hahn, 1962) Interestingly, with windowed pulses, the

16   SL profile appears similar to that with continuous pulses, and even under a low rf-field strength

17   of 1 kHz, there is no change in the SL signal intensities (Figure S1A in supplementary

18   information, SI). The experimental spin-echo(Hahn, 1950) and inversion recovery(Vold et al.,

19   1968) curves for this sample are illustrated in Figure S1A-B in SI.

20   From Figure 2, we can also observe that the location of the first minimum signal intensity in the

21   experimental SL profiles depends on the MAS rate (indicated in gray in Figure 2). For 10 kHz

22   MAS (Figure 2A and 2C), the locations are approximately at a 3 ms SL time, while for 20 kHz

23   (Figure 2D) and 35 kHz (Figure 2B), the locations are approximately at 1 ms and 0.4 ms,

1   respectively. However, in all four profiles at these minimum points, the signal reaches a similar

2   value of approximately 0.53.
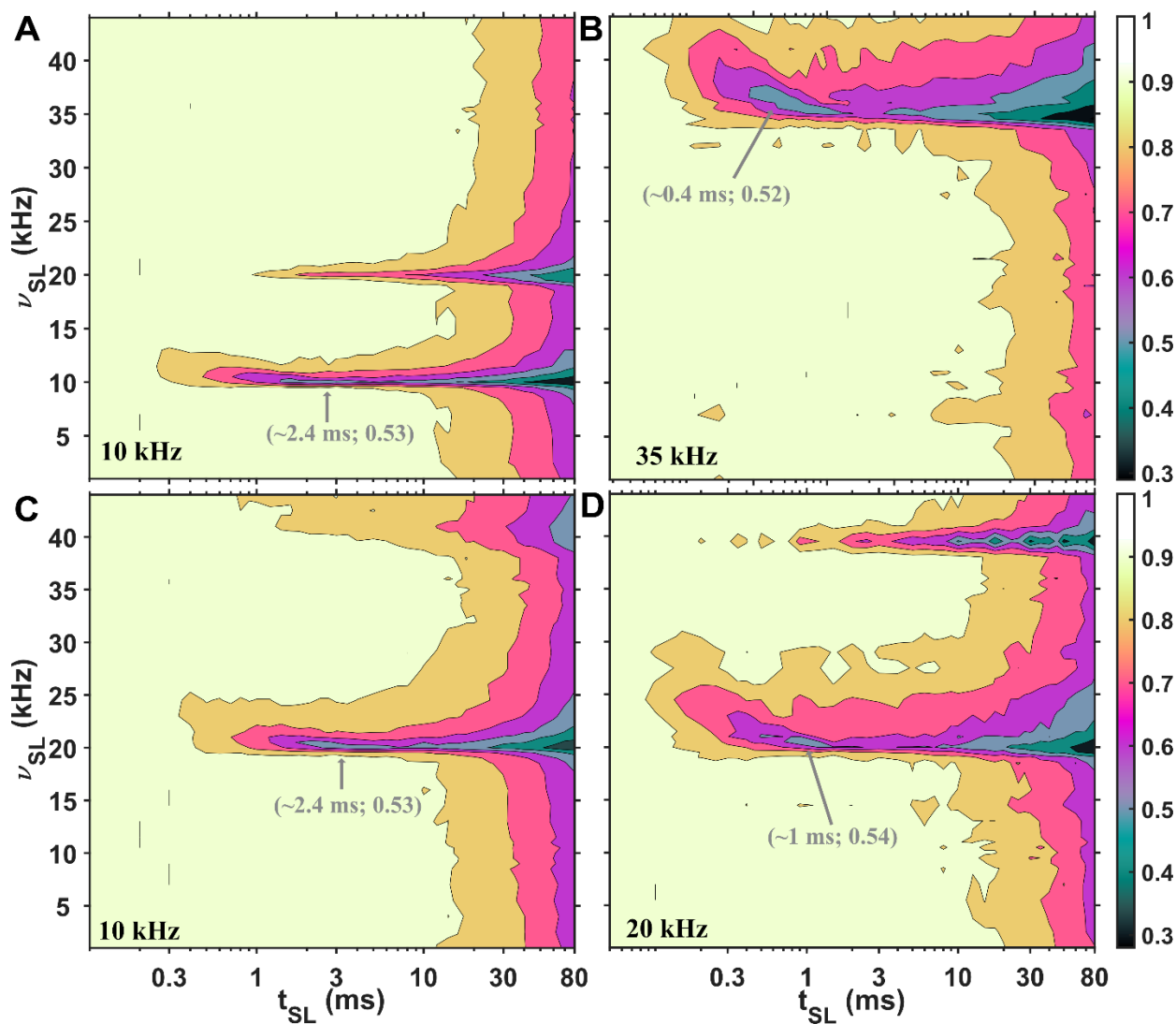
4   **Figure 2** ^{13}C polybutadiene rubber signal (the peak intensities) is shown as functions of the rf-field strength (ν_{SL}, y-

5   axis) and mixing time (t_{SL}, x-axis) of the SL under three different MAS rates: 10 kHz (A and C), 20 kHz (D) and 35

6   kHz (B). For (A), (B) and (D), continuous SL was applied, while for (C), windowed (half rotor period was filled

7   with the pulse) SL was implemented. The values in gray represent the coordinates of the first minimum in the

8   profiles. Additional experimental details are provided in the supplementary information (SI).

Rotary-resonance conditions at ν_R and $2\nu_R$ of rf-field strength are also observed for the polyethylene glycol (Figure 3B, acquired with a 4 mm probe) and for residual protons in liquid deuterium oxide samples (Figure 3D, acquired with a 1.3 mm probe). The 1D spectra of these samples are shown in Figure 3A and C, for PEG and liquid water. For each sample, two rotary-resonance conditions are observed at positions equal to integer multiplies of the MAS rates $(\nu_{SL} = \nu_R, 2\nu_R)$. For liquid water (Figure 3D), the additional rotary-resonance condition with n=3 appears very weakly. We more carefully sampled around this condition for the water sample.

The performance of the SL experiments on all three samples helps rule out the influence of translational diffusion(Hahn, 1950) (which may be present for polyethylene glycol and liquid water but not for polybutadiene rubber) or residual dipolar interaction(Cohen-Addad and Vogin, 1974) (which might be present for polybutadiene rubber but is not relevant for polyethylene glycol and liquid water).
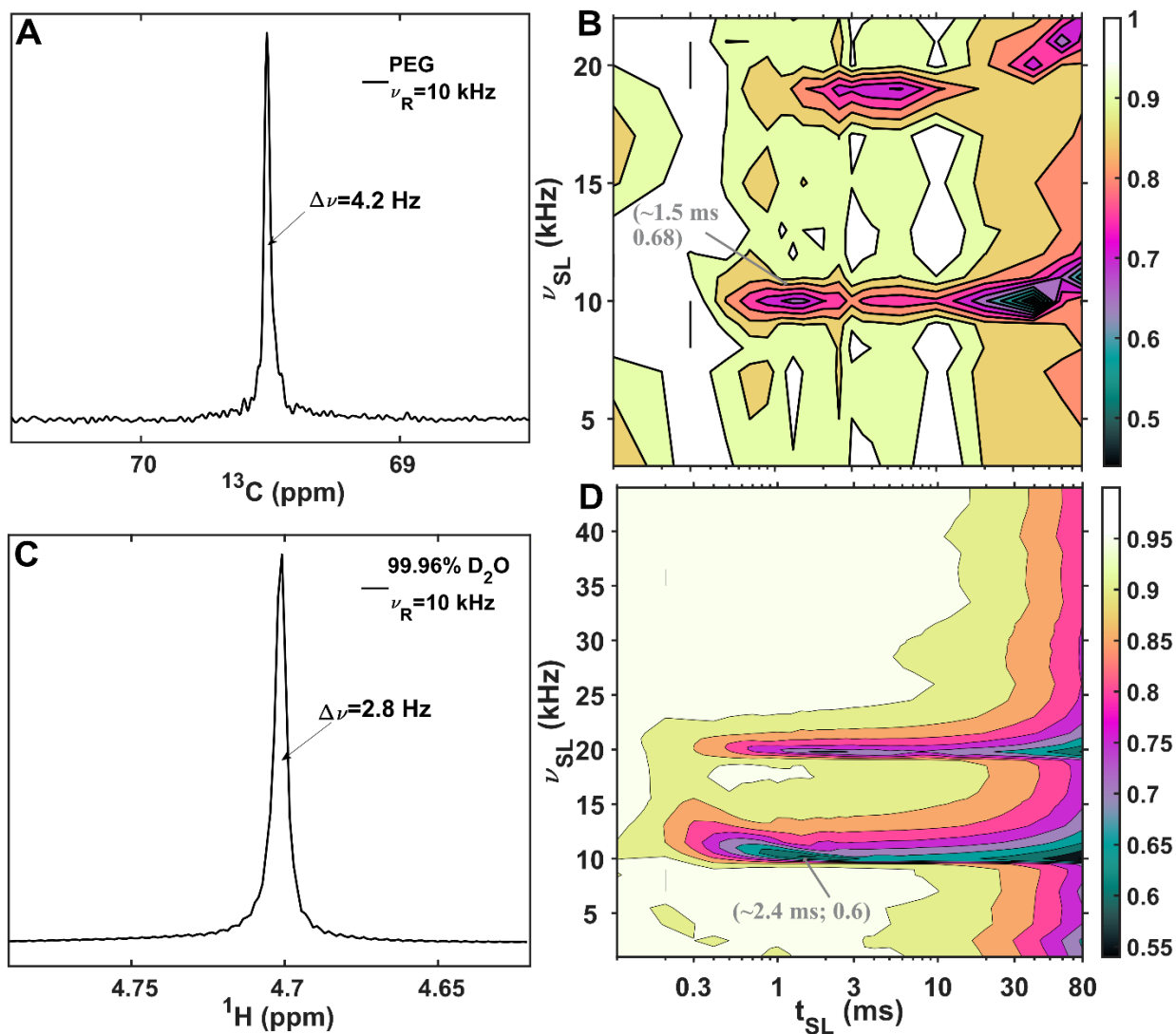
Figure 3 ^{13}C and ^{1}H spin-lock profiles at 10 kHz MAS. (A-B) Single-pulse ^{13}C spectra and SL profile of polyethylene glycol (PEG) acquired with a 4 mm probe. (C,D) ^{1}H single pulse and SL profile of 99.96% D_2O acquired with a 1.3 mm probe. The profiles in (B,D) show ^{13}C and ^{1}H signal amplitudes (peak intensities) as a function of the rf-field strength (ν_{SL}, y-axis) and mixing time (t_{SL}, x-axis) of the SL pulse. The values in gray are the coordinates of the first minimum in the profiles. Additional experimental details are provided in the supplementary information (SI).

To understand the major source of the apparent rotary-resonance conditions in liquid and liquid-like samples, we performed numerical simulations. In these simulations, two scenarios

1   were considered in which the external magnetic fields (B_0 or B_1) gained time dependence due to

2   the rotation of the sample and:

3   -   A spatially inhomogeneous external magnetic field strength (B_0 modulation),

4   -   A spatially inhomogeneous rf-field strength (B_1 modulation).

5   Note that the first scenario is compatible with a narrow linewidth under MAS.(Sodickson and

6   Cory, 1997) The specific spatial distributions chosen for B_0 and B_1, which, along with MAS,

7   introduce modulations, are summarized in Table S1 and shown in Figure S7 in SI. Additionally,

8   for each scenario, a time-independent distribution of rf-field strength was also included. Its

9   profile and influence has been investigated previously(Engelke, 2002; Gupta et al., 2015; Hoult,

10   1976; Paulson et al., 2004; Tošner et al., 2017, 2018). This type of inhomogeneity is expected for

11   solenoidal coils in which the sample near the ends of the coil experiences a lower rf-field

12   strength. For simplicity, we did not include a time-independent distribution of external magnetic

13   field strength,(Hoult, 1976; Hürlimann and Griffin, 2000) as it had a minor effect in our

14   experiments, and shimming under MAS ensures that it is minimal.

15   The effects of inhomogeneous rf-field on MAS spectra have been investigated

16   previously.(Aebischer et al., 2021; Goldman and Tekely, 2001; Tekely and Goldman, 2001;

17   Tošner et al., 2017) Rather than B_1 oscillations, the coil receptivity was shown to oscillate due to

18   rotation of the sample relative to the coil, and the authors showed that this instrumental

19   imperfection results in the appearance of sidebands that are unrelated to the chemical shift

20   anisotropy (CSA).(Goldman and Tekely, 2001; Tekely and Goldman, 2001) Sidebands due to

21   rotation through inhomogeneous B_0 and B_1 fields is a well-known effect in liquids.(Malinowski

22   and Pierpaoli, 1969; Vera and Grutzner, 1986) For solid samples, Aebischer et al.(Aebischer et

23   al., 2021) investigated the influence of time-dependent modulations of the rf-field amplitude and

phase on the performance of selected recoupling sequences and nutation experiments. In this case, the modulations did not significantly affect most recoupling sequences, with the exception of double quantum C-symmetry sequences.(Lee et al., 1995) It was noted much earlier that oscillations in phase were needed to fully explain experimental results in rotary resonance recoupling.(Levitt et al., 1988) Consistent with the matching conditions identified in this study, Aebisher et al.(Aebischer et al., 2021) revealed significant effects at ν_R and $2\nu_R$ in nutation spectra. The distribution of B_1 fields in a solenoidal coil was elegantly visualized in SL experiments of solid samples, in which case the loss of signal at rotary resonance was interpreted as CSA recoupling.(Tošner et al., 2017)

In SI, using average Hamiltonian theory(Haeberlen and Waugh, 1968) and numerical simulations, we show that the appearance of rotary-resonance conditions is primarily related to the presence of an additional time-dependent periodic term in the Hamiltonian, orthogonal to the applied RF-field spin-lock (Eqn. S1 in SI). Starting with simulations using single amplitude modulations (Figures S3-S5 in SI), we extend them to cases where these modulations have spatial distributions (Figure S6 in SI and Figures 4-5). For the qualitative determination of the source of the pseudo-RRD, we use Gaussian and bi-quadrate exponential distributions for the time-dependent and time-independent B_1 modulations, respectively (summarized in Table S1 and shown in Figure S7 in SI). While knowing the exact values and shapes of these modulations is important for quantitatively assessing their influence, these values and shapes primarily broaden the rotary-resonance conditions and affect the frequency and amplitude of the modulations in the spin-lock signals. However, they do not affect the occurrence of the rotary-resonance conditions. Consequently, rotary-resonance conditions are observed at the same MAS frequencies for both single (Figure S5 in SI) and distributed (Figure S6 in SI) B_1 modulations.

Figure 4 shows simulations for the first scenario (B$_0$ modulation). While some similarities

between Figure 2 and Figure 4 are observed, there are three major differences in the SL profiles,

which should be highlighted. Firstly, in Figure 4, the intensities at the first minima show a

dependence on MAS rate (marked in gray in Figure 4), whereas in Figure 2, the experimental

profiles show only a slight dependence. Secondly, in Figure 4, the locations of these minima in

time (x-axis) do not depend on the MAS rate (Figure $4A$, $4B$ and $4D$), whereas the location in

time changes when windowed pulses are applied (Figure $4C$). In contrast, the experimental

profiles exhibit the reverse behavior. Thirdly, in Figure $4C$, second rotary-resonance condition is

slightly observed, compared to Figures 4A and D, while in Figure 2C, two rotary-resonance

conditions are clearly detected. Additionally, increasing the magnetic field inhomogeneity by

deliberately mis-setting the room temperature shims had little influence on the SL profile (shown

in Figure $S2$ in the SI).

All of this indicates that a spatially inhomogeneous external magnetic field cannot be a major

source of the appearance of rotary-resonances conditions in rotating liquids and liquid-like

samples.
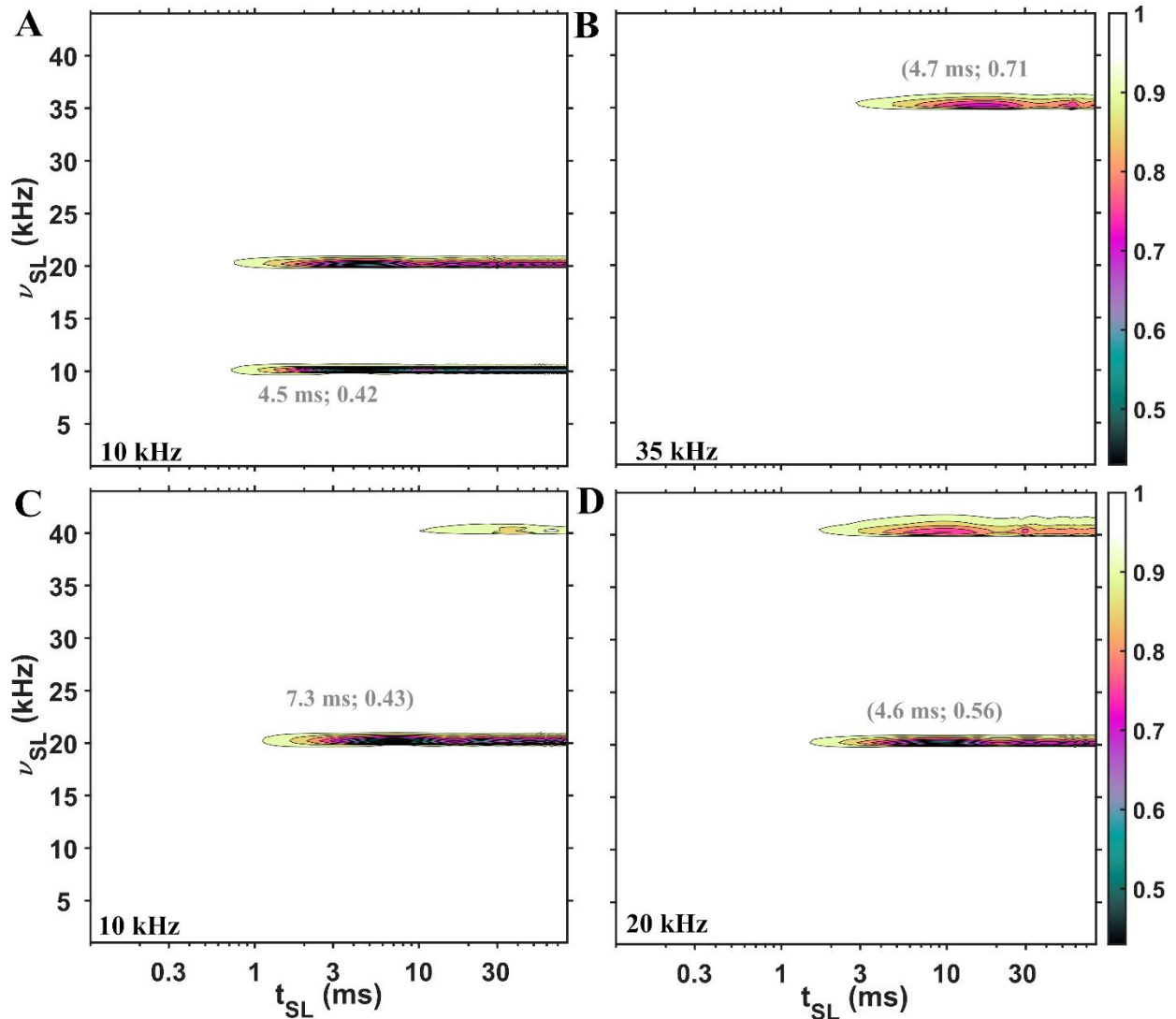
Figure 4 Simulated SL profiles showing the influence of time dependence introduced via an inhomogeneous

external magnetic field. The simulated signal is shown as a function of the rf-field strength (ν_{SL}, axis y) and mixing

time (t_{SL}, axis x) of the SL under three different MAS rates: 10 kHz (A and C), 20 kHz (D) and 35 kHz (B). For (A),

(B) and (D), continuous SL was applied, while for (C) windowed SL was implemented (half rotor period was filled

with the pulse). The values in gray represent the coordinates of the first minima in the profiles. No

phenomenological relaxation was included in the simulations. Additional simulated details are provided in the SI.

In contrast, simulations of SL profiles with time dependence introduced via a spatially

inhomogeneous rf-field (Figure 5, B₁ modulation) qualitatively agree with the experimental

plots, indicating that a spatially inhomogeneous rf-field is a better explanation for the appearance

of rotary-resonance conditions in rotating liquids and liquid-like samples using conventional MAS NMR probes with solenoidal coils. Such time dependence has been previously considered in the design of magnetization transfer elements using optimal control.(Blahut et al., 2022, 2023; Glaser et al., 2015; Joseph and Griesinger, 2023; Tošner et al., 2017, 2018)

This qualitative explanation, provided by simulations, indicates that this effect can also be anticipated in experiments involving solid samples, in addition to the desired effects caused by molecular motion. It is therefore recommended to consider coil inhomogeneity when measuring relaxation rates near rotary resonance conditions. Fortunately, the magnitude of this effect is considerably smaller than the strong relaxation observed in recent reports that detected slow structural dynamics via near rotary resonance conditions.(Krushelnitsky et al., 2018)
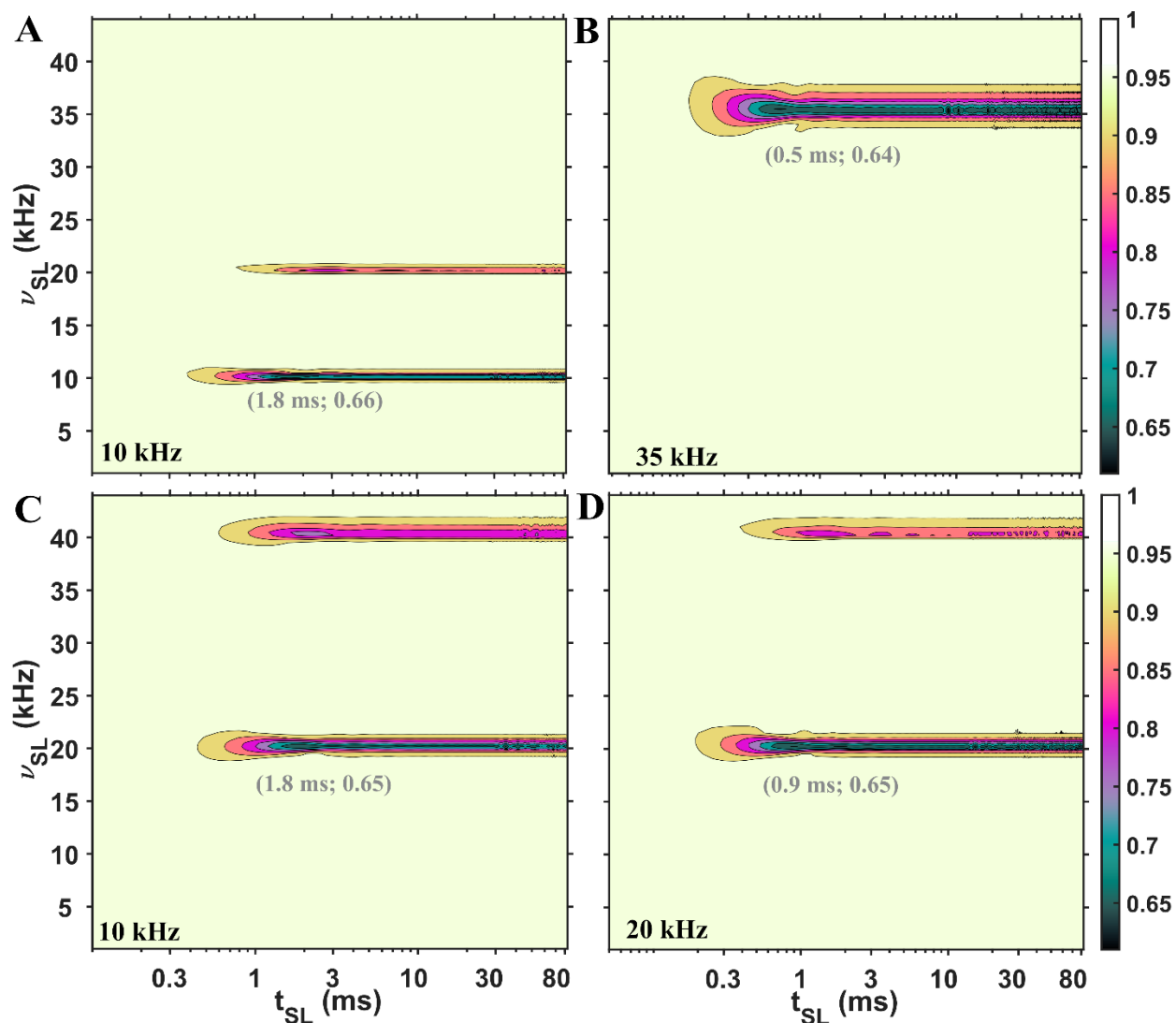
Figure 5 The influence of the inhomogeneous rf-field on the simulated SL profiles. The simulated signal is shown as functions of the rf-field strength (ν_{SL}, axis y) and mixing time (t_{SL}, axis x) of the SL under three different MAS rates: 10 kHz (A and C), 20 kHz (D) and 35 kHz (B). For (A), (B) and (D), continuous SL was applied, while for (C) windowed (half rotor period was filled with the pulse) SL was implemented. The values in gray represent the coordinates of the first minima points in the profiles. Relaxation was not included in the simulations. Additional simulated details are provided in the SI.

Conclusions

Rotary-resonance conditions, under which the applied rf-field strength equals an even multiple of the MAS rate, provide a powerful avenue to obtain specific structural information via recoupling of anisotropic interactions in solids(De Paëpe, 2012; Nishiyama et al., 2022) or for detecting changes in the relaxation rates due to slow motion in the μs range.(Rovó, 2020) Canonically, rotary-resonance conditions are not expected in liquids due to the averaging of first-order anisotropic interactions from (sub) nanosecond isotropic motion.(Haeberlen and Waugh, 1968; Maricq, 1982) In this article, we presented experimental data, in which we detected rotary-resonance conditions in a liquid and a liquid-like samples. We qualitatively explained the major source of these conditions, which can occur from a combination of two factors: the rotation of the sample and a spatially inhomogeneous rf-field produced a solenoidal coil.(Tošner et al., 2017) As a result, the rf-field Hamiltonian contains time-dependent terms, which leads to signal decrease, i.e. pseudo relaxation behavior, at or near rotary-resonance conditions. To mitigate these effects, it may be advantageous to consider different hardware designs,(Chen et al., 2018; Xu et al., 2021) for example rf coils that produce more homogeneous rf-fields.(Grant et al., 2010; Kelz et al., 2019; Krahn et al., 2008; Stringer et al., 2005)

Competing interests

The contact author has declared that none of the authors has any competing interests.

Acknowledgments

We acknowledge financial support from the MPI for Multidisciplinary Sciences, and from the Deutsche Forschungsgemeinschaft (Emmy Noether program Grant AN1316/1-2). We thank Dr. Supriya Pratihar for inspiring this work by noticing pseudo-RRD at rotary resonance conditions in exploratory high-power relaxation dispersion measurements in a 0.7 mm MAS probe. We thank Dr. Dirk Bockelmann and Brigitta Angerstein for technical assistance.

1 **Author contribution**

2 EN and LBA designed the experiments. EN and JM recorded NMR data and ran simulations, EN

3 and LBA wrote the article. All authors edited and approved the article.

4 **References**

5 Abyzov, A., Blackledge, M., and Zweckstetter, M.: Conformational Dynamics of Intrinsically Disordered
6 Proteins Regulate Biomolecular Condensate Chemistry, Chem. Rev., 122, 6719–6748,
7 https://doi.org/10.1021/acs.chemrev.1c00774, 2022.

8 Aebischer, K., Tošner, Z., and Ernst, M.: Effects of radial radio-frequency field inhomogeneity on MAS
9 solid-state NMR experiments, Magn. Reson., 2, 523–543, https://doi.org/10.5194/mr-2-523-2021, 2021.

10 Alam, M. K., Bhuvaneshwari, R. A., and Sengupta, I.: 19F NMR relaxation of buried tryptophan side
11 chains suggest anisotropic rotational diffusion of the protein RfaH, J. Biomol. NMR,
12 https://doi.org/10.1007/s10858-024-00450-x, 2024.

13 Andrew, E. R., Bradbury, A., and Eades, R. G.: Nuclear Magnetic Resonance Spectra from a Crystal
14 rotated at High Speed, Nature, 182, 1659–1659, https://doi.org/10.1038/1821659a0, 1958.

15 Blahut, J., Brandl, M. J., Pradhan, T., Reif, B., and Tošner, Z.: Sensitivity-Enhanced Multidimensional
16 Solid-State NMR Spectroscopy by Optimal-Control-Based Transverse Mixing Sequences, J. Am. Chem.
17 Soc., https://doi.org/10.1021/jacs.2c06568, 2022.

18 Blahut, J., Brandl, M. J., Sarkar, R., Reif, B., and Tošner, Z.: Optimal control derived sensitivity-enhanced
19 CA-CO mixing sequences for MAS solid-state NMR – Applications in sequential protein backbone
20 assignments, J. Magn. Reson. Open, 16–17, 100122, https://doi.org/10.1016/j.jmro.2023.100122, 2023.

21 Camacho-Zarco, A. R., Schnapka, V., Guseva, S., Abyzov, A., Adamski, W., Milles, S., Jensen, M. R., Zidek,
22 L., Salvi, N., and Blackledge, M.: NMR Provides Unique Insight into the Functional Dynamics and
23 Interactions of Intrinsically Disordered Proteins, Chem. Rev., 122, 9331–9356,
24 https://doi.org/10.1021/acs.chemrev.1c01023, 2022.

25 Cavanagh, J., Fairbrother, W. J., Palmer, A. G., III., Rance, M., and Skelton, N. J.: Protein NMR
26 Spectroscopy: Principles and Practice, 1 pp., 2006.

27 Chen, P., Albert, B. J., Gao, C., Alaniva, N., Price, L. E., Scott, F. J., Saliba, E. P., Sesti, E. L., Judge, P. T.,
28 Fisher, E. W., and Barnes, A. B.: Magic angle spinning spheres, Sci. Adv., 4, eaau1540,
29 https://doi.org/10.1126/sciadv.aau1540, 2018.

30 Cohen-Addad, J. P. and Vogin, R.: Molecular Motion Anisotropy as Reflected by a "Pseudosolid" Nuclear
31 Spin Echo: Observation of Chain Constraints in Molten cis-1, 4-Polybutadiene, Phys. Rev. Lett., 33, 940–
32 943, https://doi.org/10.1103/PhysRevLett.33.940, 1974.

1 De Paëpe, G.: Dipolar Recoupling in Magic Angle Spinning Solid-State Nuclear Magnetic Resonance,
2 Annu. Rev. Phys. Chem., 63, 661–684, https://doi.org/10.1146/annurev-physchem-032511-143726,
3 2012.

4 Deverell, C., Morgan, R. E., and Strange, J. H.: Studies of chemical exchange by nuclear magnetic
5 relaxation in the rotating frame, Mol. Phys., 18, 553–559, https://doi.org/10.1080/00268977000100611,
6 1970.

7 Engelke, F.: Electromagnetic wave compression and radio frequency homogeneity in NMR solenoidal
8 coils: Computational approach, Concepts Magn. Reson., 15, 129–155,
9 https://doi.org/10.1002/cmr.10029, 2002.

10 Fonseca, R., Vieira, R., Sardo, M., Marin-Montesinos, I., and Mafra, L.: Exploring Molecular Dynamics of
11 Adsorbed CO_2 Species in Amine-Modified Porous Silica by Solid-State NMR Relaxation, J. Phys. Chem. C,
12 126, 12582–12591, https://doi.org/10.1021/acs.jpcc.2c02656, 2022.

13 Furman, G. B., Panich, A. M., and Goren, S. D.: Spin-locking in one pulse NMR experiment, Solid State
14 Nucl. Magn. Reson., 11, 225–230, https://doi.org/10.1016/S0926-2040(97)00108-2, 1998.

15 Glaser, S. J., Boscain, U., Calarco, T., Koch, C. P., Köckenberger, W., Kosloff, R., Kuprov, I., Luy, B.,
16 Schirmer, S., Schulte-Herbrüggen, T., Sugny, D., and Wilhelm, F. K.: Training Schrödinger's cat: quantum
17 optimal control, Eur. Phys. J. D, 69, 279, https://doi.org/10.1140/epjd/e2015-60464-1, 2015.

18 Goldman, M. and Tekely, P.: Effect of radial RF field on MAS spectra, Comptes Rendus Académie Sci. -
19 Ser. IIC - Chem., 4, 795–800, https://doi.org/10.1016/S1387-1609(01)01310-X, 2001.

20 Grant, C. V., Wu, C. H., and Opella, S. J.: Probes for high field solid-state NMR of lossy biological samples,
21 J. Magn. Reson., 204, 180–188, https://doi.org/10.1016/j.jmr.2010.03.011, 2010.

22 Gupta, R., Hou, G., Polenova, T., and Vega, A. J.: RF Inhomogeneity and how it Control CPMAS, Solid
23 State Nucl. Magn. Reson., 72, 17–26, https://doi.org/10.1016/j.ssnmr.2015.09.005, 2015.

24 Haeberlen, U. and Waugh, J. S.: Coherent Averaging Effects in Magnetic Resonance, Phys. Rev., 175,
25 453–467, https://doi.org/10.1103/PhysRev.175.453, 1968.

26 Hahn, E. L.: Spin Echoes, Phys. Rev., 80, 580–594, https://doi.org/10.1103/PhysRev.80.580, 1950.

27 Hartmann, S. R. and Hahn, E. L.: Nuclear Double Resonance in the Rotating Frame, Phys. Rev., 128,
28 2042–2053, https://doi.org/10.1103/PhysRev.128.2042, 1962.

29 Hoult, D. I.: Solvent peak saturation with single phase and quadrature fourier transformation, J. Magn.
30 Reson. 1969, 21, 337–347, https://doi.org/10.1016/0022-2364(76)90081-0, 1976.

31 Hu, Y., Cheng, K., He, L., Zhang, X., Jiang, B., Jiang, L., Li, C., Wang, G., Yang, Y., and Liu, M.: NMR-Based
32 Methods for Protein Analysis, Anal. Chem., 93, 1866–1879,
33 https://doi.org/10.1021/acs.analchem.0c03830, 2021.

1 Hürlimann, M. D. and Griffin, D. D.: Spin Dynamics of Carr–Purcell–Meiboom–Gill-like Sequences in
2 Grossly Inhomogeneous B_0 and B_1 Fields and Application to NMR Well Logging, J. Magn. Reson., 143,
3 120–135, https://doi.org/10.1006/jmre.1999.1967, 2000.

4 Joseph, D. and Griesinger, C.: Optimal control pulses for the 1.2-GHz (28.2-T) NMR spectrometers, Sci.
5 Adv., 9, eadj1133, https://doi.org/10.1126/sciadv.adj1133, 2023.

6 Keeler, E. G. and McDermott, A. E.: Rotating Frame Relaxation in Magic Angle Spinning Solid State NMR,
7 a Promising Tool for Characterizing Biopolymer Motion, Chem. Rev., 122, 14940–14953,
8 https://doi.org/10.1021/acs.chemrev.2c00442, 2022.

9 Kelz, J. I., Kelly, J. E., and Martin, R. W.: 3D-printed dissolvable inserts for efficient and customizable
10 fabrication of NMR transceiver coils, J. Magn. Reson., 305, 89–92,
11 https://doi.org/10.1016/j.jmr.2019.06.008, 2019.

12 Krahn, A., Priller, U., Emsley, L., and Engelke, F.: Resonator with reduced sample heating and increased
13 homogeneity for solid-state NMR, J. Magn. Reson., 191, 78–92,
14 https://doi.org/10.1016/j.jmr.2007.12.004, 2008.

15 Krushelnitsky, A., Gauto, D., Rodriguez Camargo, D. C., Schanda, P., and Saalwächter, K.: Microsecond
16 motions probed by near-rotary-resonance R1ρ 15N MAS NMR experiments: the model case of protein
17 overall-rocking in crystals, J. Biomol. NMR, 71, 53–67, https://doi.org/10.1007/s10858-018-0191-4,
18 2018.

19 Krushelnitsky, A., Hempel, G., Jurack, H., and Mendes Ferreira, T.: Rocking motion in solid proteins
20 studied by the 15 N proton-decoupled R 1ρ relaxometry, Phys. Chem. Chem. Phys., 25, 15885–15896,
21 https://doi.org/10.1039/D3CP00444A, 2023.

22 Kupče, Ē., Keifer, P. A., and Delepierre, M.: Adiabatic TOCSY MAS in Liquids, J. Magn. Reson., 148, 115–
23 120, https://doi.org/10.1006/jmre.2000.2224, 2001.

24 Kurauskas, V., Izmailov, S. A., Rogacheva, O. N., Hessel, A., Ayala, I., Woodhouse, J., Shilova, A., Xue, Y.,
25 Yuwen, T., Coquelle, N., Colletier, J.-P., Skrynnikov, N. R., and Schanda, P.: Slow conformational
26 exchange and overall rocking motion in ubiquitin protein crystals, Nat. Commun., 8, 145,
27 https://doi.org/10.1038/s41467-017-00165-8, 2017.

28 Kurbanov, R., Zinkevich, T., and Krushelnitsky, A.: The nuclear magnetic resonance relaxation data
29 analysis in solids: General R 1/ R 1 ρ equations and the model-free approach, J. Chem. Phys., 135,
30 184104, https://doi.org/10.1063/1.3658383, 2011.

31 Lee, Y. K., Kurur, N. D., Helmle, M., Johannessen, O. G., Nielsen, N. C., and Levitt, M. H.: Efficient dipolar
32 recoupling in the NMR of rotating solids. A sevenfold symmetric radiofrequency pulse sequence, Chem.
33 Phys. Lett., 242, 304–309, https://doi.org/10.1016/0009-2614(95)00741-L, 1995.

34 Levitt, M. H., Oas, T. G., and Griffin, R. G.: Rotary Resonance Recoupling in Heteronuclear Spin Pair
35 Systems, Isr. J. Chem., 28, 271–282, https://doi.org/10.1002/ijch.198800039, 1988.

1   Lewandowski, J. R., Sass, H. J., Grzesiek, S., Blackledge, M., and Emsley, L.: Site-Specific Measurement of
2   Slow Motions in Proteins, J. Am. Chem. Soc., 133, 16762–16765, https://doi.org/10.1021/ja206815h,
3   2011.

4   Lowe, I. J.: Free Induction Decays of Rotating Solids, Phys. Rev. Lett., 2, 285–287,
5   https://doi.org/10.1103/PhysRevLett.2.285, 1959.

6   Ma, P., Haller, J. D., Zajakala, J., Macek, P., Sivertsen, A. C., Willbold, D., Boisbouvier, J., and Schanda, P.:
7   Probing Transient Conformational States of Proteins by Solid-State R1ρ Relaxation-Dispersion NMR
8   Spectroscopy, Angew. Chem. Int. Ed., 53, 4312–4317, https://doi.org/10.1002/anie.201311275, 2014.

9   Malinowski, E. R. and Pierpaoli, A. R.: Asymmetric spinning sidebands from coaxial cells in NMR spectra,
10 J. Magn. Reson. 1969, 1, 509–515, https://doi.org/10.1016/0022-2364(69)90087-0, 1969.

11 Maricq, M. M.: Application of average Hamiltonian theory to the NMR of solids, Phys. Rev. B, 25, 6622–
12 6632, https://doi.org/10.1103/PhysRevB.25.6622, 1982.

13 Marion, D., Gauto, D. F., Ayala, I., Giandoreggio-Barranco, K., and Schanda, P.: Microsecond Protein
14 Dynamics from Combined Bloch-McConnell and Near-Rotary-Resonance R1 Relaxation-Dispersion MAS
15 NMR, ChemPhysChem, 20, 276–284, https://doi.org/10.1002/cphc.201800935, 2019.

16 Massi, F. and Peng, J. W.: Characterizing Protein Dynamics with NMR R1ρRelaxation Experiments, in:
17 Protein NMR: Methods and Protocols, edited by: Ghose, R., Springer, New York, NY, 205–221,
18 https://doi.org/10.1007/978-1-4939-7386-6_10, 2018.

19 Nimerovsky, E. and Goldbourt, A.: Insights into the spin dynamics of a large anisotropy spin subjected to
20 long-pulse irradiation under a modified REDOR experiment, J. Magn. Reson., 225, 130–141,
21 https://doi.org/10.1016/j.jmr.2012.09.015, 2012.

22 Nimerovsky, E., Becker, S., and Andreas, L. B.: Windowed cross polarization at 55 kHz magic-angle
23 spinning, J. Magn. Reson., 349, 107404, https://doi.org/10.1016/j.jmr.2023.107404, 2023.

24 Nishiyama, Y., Hou, G., Agarwal, V., Su, Y., and Ramamoorthy, A.: Ultrafast Magic Angle Spinning Solid-
25 State NMR Spectroscopy: Advances in Methodology and Applications, Chem. Rev.,
26 https://doi.org/10.1021/acs.chemrev.2c00197, 2022.

27 Oas, T. G., Griffin, R. G., and Levitt, M. H.: Rotary resonance recoupling of dipolar interactions in solid-
28 state nuclear magnetic resonance spectroscopy, J. Chem. Phys., 89, 692–695,
29 https://doi.org/10.1063/1.455191, 1988.

30 Öster, C., Kosol, S., and Lewandowski, J. R.: Quantifying Microsecond Exchange in Large Protein
31 Complexes with Accelerated Relaxation Dispersion Experiments in the Solid State, Sci. Rep., 9, 11082,
32 https://doi.org/10.1038/s41598-019-47507-8, 2019.

33 Palmer, A. G. and Massi, F.: Characterization of the Dynamics of Biomacromolecules Using Rotating-
34 Frame Spin Relaxation NMR Spectroscopy, Chem. Rev., 106, 1700–1719,
35 https://doi.org/10.1021/cr0404287, 2006.

1   Palmer, A. G. I.: NMR Characterization of the Dynamics of Biomacromolecules, Chem. Rev., 104, 3623–
2   3640, https://doi.org/10.1021/cr030413t, 2004.

3   Palmer, A. G. I.: Enzyme Dynamics from NMR Spectroscopy, Acc. Chem. Res., 48, 457–465,
4   https://doi.org/10.1021/ar500340a, 2015.

5   Paulson, E. K., Martin, R. W., and Zilm, K. W.: Cross polarization, radio frequency field homogeneity, and
6   circuit balancing in high field solid state NMR probes, J. Magn. Reson., 171, 314–323,
7   https://doi.org/10.1016/j.jmr.2004.09.009, 2004.

8   Pratihar, S., Sabo, T. M., Ban, D., Fenwick, R. B., Becker, S., Salvatella, X., Griesinger, C., and Lee, D.:
9   Kinetics of the Antibody Recognition Site in the Third IgG-Binding Domain of Protein G, Angew. Chem.
10   Int. Ed., 55, 9567–9570, https://doi.org/10.1002/anie.201603501, 2016.

11   Quinn, C. M. and McDermott, A. E.: Monitoring conformational dynamics with solid-state $R1\rho$
12   experiments, J. Biomol. NMR, 45, 5–8, https://doi.org/10.1007/s10858-009-9346-7, 2009.

13   Rangadurai, A., Szymaski, E. S., Kimsey, I. J., Shi, H., and Al-Hashimi, H. M.: Characterizing micro-to-
14   millisecond chemical exchange in nucleic acids using off-resonance $R1\rho$ relaxation dispersion, Prog. Nucl.
15   Magn. Reson. Spectrosc., 112–113, 55–102, https://doi.org/10.1016/j.pnmrs.2019.05.002, 2019.

16   Redfield, A. G.: On the Theory of Relaxation Processes, IBM J. Res. Dev., 1, 19–31,
17   https://doi.org/10.1147/rd.11.0019, 1957.

18   Rovó, P.: Recent advances in solid-state relaxation dispersion techniques, Solid State Nucl. Magn.
19   Reson., 108, 101665, https://doi.org/10.1016/j.ssnmr.2020.101665, 2020.

20   Rovó, P. and Linser, R.: Microsecond Timescale Protein Dynamics: a Combined Solid-State NMR
21   Approach, ChemPhysChem, 19, 34–39, https://doi.org/10.1002/cphc.201701238, 2018.

22   Schanda, P. and Ernst, M.: Studying dynamics by magic-angle spinning solid-state NMR spectroscopy:
23   Principles and applications to biomolecules, Prog. Nucl. Magn. Reson. Spectrosc., 96, 1–46,
24   https://doi.org/10.1016/j.pnmrs.2016.02.001, 2016.

25   Schmidt-Rohr, K., Clauss, J., and Spiess, H. W.: Correlation of structure, mobility, and morphological
26   information in heterogeneous polymer materials by two-dimensional wideline-separation NMR
27   spectroscopy, Macromolecules, 25, 3273–3277, https://doi.org/10.1021/ma00038a037, 1992.

28   Sekhar, A. and Kay, L. E.: An NMR View of Protein Dynamics in Health and Disease, Annu. Rev. Biophys.,
29   48, 297–319, https://doi.org/10.1146/annurev-biophys-052118-115647, 2019.

30   Shaka, A. J., Keeler, J., Frenkiel, T., and Freeman, R.: An improved sequence for broadband decoupling:
31   WALTZ-16, J. Magn. Reson. 1969, 52, 335–338, https://doi.org/10.1016/0022-2364(83)90207-X, 1983.

32   Shcherbakov, A. A., Brousseau, M., Henzler-Wildman, K. A., and Hong, M.: Microsecond Motion of the
33   Bacterial Transporter EmrE in Lipid Bilayers, J. Am. Chem. Soc., 145, 10104–10115,
34   https://doi.org/10.1021/jacs.3c00340, 2023.

1   Sodickson, A. and Cory, D. G.: Shimming a High-Resolution MAS Probe, J. Magn. Reson., 128, 87–91,
2   https://doi.org/10.1006/jmre.1997.1218, 1997.

3   Stief, T., Vormann, K., and Lakomek, N.-A.: Sensitivity-enhanced NMR 15N R1 and R1ρ relaxation
4   experiments for the investigation of intrinsically disordered proteins at high magnetic fields, Methods,
5   223, 1–15, https://doi.org/10.1016/j.ymeth.2024.01.008, 2024.

6   Stringer, J. A., Bronnimann, C. E., Mullen, C. G., Zhou, D. H., Stellfox, S. A., Li, Y., Williams, E. H., and
7   Rienstra, C. M.: Reduction of RF-induced sample heating with a scroll coil resonator structure for solid-
8   state NMR probes, J. Magn. Reson., 173, 40–48, https://doi.org/10.1016/j.jmr.2004.11.015, 2005.

9   Tekely, P. and Goldman, M.: Radial-Field Sidebands in MAS, J. Magn. Reson., 148, 135–141,
10 https://doi.org/10.1006/jmre.2000.2215, 2001.

11 Tošner, Z., Purea, A., Struppe, J. O., Wegner, S., Engelke, F., Glaser, S. J., and Reif, B.: Radiofrequency
12 fields in MAS solid state NMR probes, J. Magn. Reson., 284, 20–32,
13 https://doi.org/10.1016/j.jmr.2017.09.002, 2017.

14 Tošner, Z., Sarkar, R., Becker-Baldus, J., Glaubitz, C., Wegner, S., Engelke, F., Glaser, S. J., and Reif, B.:
15 Overcoming Volume Selectivity of Dipolar Recoupling in Biological Solid-State NMR Spectroscopy,
16 Angew. Chem. Int. Ed., 57, 14514–14518, https://doi.org/10.1002/anie.201805002, 2018.

17 Vera, Marisol. and Grutzner, J. B.: The Taylor vortex: the measurement of viscosity in NMR samples, J.
18 Am. Chem. Soc., 108, 1304–1306, https://doi.org/10.1021/ja00266a035, 1986.

19 Vold, R. L., Waugh, J. S., Klein, M. P., and Phelps, D. E.: Measurement of Spin Relaxation in Complex
20 Systems, J. Chem. Phys., 48, 3831–3832, https://doi.org/10.1063/1.1669699, 1968.

21 Vugmeyster, L., Ostrovsky, D., Greenwood, A., and Fu, R.: Deuteron rotating frame relaxation for the
22 detection of slow motions in rotating solids, J. Magn. Reson., 337, 107171,
23 https://doi.org/10.1016/j.jmr.2022.107171, 2022.

24 Vugmeyster, L., Rodgers, A., Ostrovsky, D., James McKnight, C., and Fu, R.: Deuteron off-resonance
25 rotating frame relaxation for the characterization of slow motions in rotating and static solid-state
26 proteins, J. Magn. Reson., 352, 107493, https://doi.org/10.1016/j.jmr.2023.107493, 2023.

27 Wang, A. C. and Bax, A.: Minimizing the effects of radio-frequency heating in multidimensional NMR
28 experiments, J. Biomol. NMR, 3, 715–720, https://doi.org/10.1007/BF00198374, 1993.

29 Xu, K., Pecher, O., Braun, M., and Schmedt auf der Günne, J.: Stable magic angle spinning with Low-Cost
30 3D-Printed parts, J. Magn. Reson., 333, 107096, https://doi.org/10.1016/j.jmr.2021.107096, 2021.

31 Zektzer, A. S., Swanson, M. G., Jarso, S., Nelson, S. J., Vigneron, D. B., and Kurhanewicz, J.: Improved
32 signal to noise in high-resolution magic angle spinning total correlation spectroscopy studies of prostate
33 tissues using rotor-synchronized adiabatic pulses, Magn. Reson. Med., 53, 41–48,
34 https://doi.org/10.1002/mrm.20335, 2005.

35